

High extinction ratio thermo-optic based reconfigurable optical logic gates for programmable PICs

Cite as: AIP Advances 12, 055304 (2022); <https://doi.org/10.1063/5.0086185>

Submitted: 26 February 2022 • Accepted: 11 April 2022 • Published Online: 03 May 2022

S. Hassan,  D. Chack and  L. Pavesi



View Online



Export Citation



CrossMark



High extinction ratio thermo-optic based reconfigurable optical logic gates for programmable PICs

Cite as: AIP Advances 12, 055304 (2022); doi: 10.1063/5.0086185

Submitted: 26 February 2022 • Accepted: 11 April 2022 •

Published Online: 3 May 2022





View Online



Export Citation



CrossMark

S. Hassan,¹ D. Chack,^{1,a)}  and L. Pavesi² 

AFFILIATIONS

¹ Department of Electronics Engineering, Indian Institute of Technology (ISM), Dhanbad 826004, India

² Nanoscience Laboratory, University of Trento, Trento 38123, Italy

^{a)} Author to whom correspondence should be addressed: devendra@iitism.ac.in

ABSTRACT

In this paper, a new scheme is proposed to realize reconfigurable and multifunction optical logic gates (XOR, XNOR, NAND, and OR) using a Mach–Zehnder interferometer with a tunable thermo-optic phase shifter (TOPS). The reconfigurable optical logic gates are realized by tuning the phase of an optical signal using TOPS without changing the physical device structure. The logical input “0” or “1” is considered corresponding to the phase of the optical signal at TOPS. The logical output of the proposed device depends on the light intensity at output ports. The device is designed on silicon on insulator (SOI) platform and the simulation result shows that the on–off extinction ratio is greater than 37 dB at 1550 nm and >25 dB for the C-band. Moreover, it has a low insertion loss of 0.09 dB at a wavelength of 1550 nm and <0.8 dB for the C-band window. The proposed optical logic gates can be a promising logical device for programmable photonic integrated circuits.

© 2022 Author(s). All article content, except where otherwise noted, is licensed under a Creative Commons Attribution (CC BY) license (<http://creativecommons.org/licenses/by/4.0/>). <https://doi.org/10.1063/5.0086185>

I. INTRODUCTION

Programmable photonic integrated circuits (PICs) are a promising technology for high performance optical computing that requires reconfigurable devices, such as tunable couplers, phase shifters, and waveguide meshes.¹ All-optical devices, such as optical splitters,² optical switches,³ and optical logic gates,⁴ are fundamental components in optical computing and signal processing. These optical components are implemented in photonic integrated circuits to overcome the limitations of electronic components, such as the speed, bandwidth, and power consumption. Silicon photonics is a suitable platform for integrating all-optical components into a single chip.⁵ The advancement in the fabrication of silicon nano-photon devices leads to high optical confinement, low losses, and complementary metal–oxide–semiconductor (CMOS) compatibility with electronics devices. Recently, the optical logic devices have been widely demonstrated for various applications, such as programmable logic arrays,⁶ nanowire networks,⁷ and optical computing.⁸ Optical computing is a significant research area

that requires high performance optical signal processing and optical logical operations.^{9,10} The 2×2 optical gate is used to couple the modulated optical signal and control the power coupling in programmable photonic circuits.¹¹ Optical logic gates can be implemented as multi-operand for optical computing¹² and for $N \times N$ unitary transformation in quantum computing.¹³ Optical logic gates have been realized using various techniques having different device structures, such as semiconductor optical amplifiers,¹⁴ microring resonators on silicon nitride,¹⁵ ring resonators with graphene nanoribbons,¹⁶ hybrid plasmonic waveguides,^{17,18} cross-phase modulation effects on phase-shifted grating,¹⁹ 2D non-linear photonic crystals using nonlinear Kerr effects,²⁰ the multimode interference (MMI) coupler with photonic crystals,²¹ and MMI using binary-phase shift-keyed signals.^{22,23} In the literature, optical logic gates have been reported using the electro-optic principle.^{24–26} While this effect yields fast switching and energy-efficient devices, the related free carrier absorption causes additional loss and crosstalk. However, we propose to use the thermo-optic effect to minimize the insertion loss and enhance the device's extinction ratio, and also

silicon has a high thermo-optic coefficient and ease of fabrication.²⁶ The previously reported MMI-based optical logic gates require multiple optical signals and a binary phase-shift keyed signal at the input to realize logic “0” and “1.” However, instead of multiple optical signals (multilaser sources) and the phase-shifted signal at the input waveguide, we have employed a single optical signal input with a tunable phase shifter at the arms of the MMI-based Mach–Zehnder interferometer (MZI) to provide logical inputs. The phase of the optical signal is tuned using the thermo-optic phase shifter (TOPS) to realize other logic gates, and also two logic gates are realized simultaneously. The proposed logic gates work as a reconfigurable and multifunction logic device.

In this article, reconfigurable and multifunction MMI-based optical logic gates have been realized using the thermo-optic principle. The TOPS are implemented on a silicon waveguide to control the phase of an optical signal to obtain a specific logic gate without changing the device structure. The logical input “0” or “1” is assumed with respect to a phase shift of the optical signal at the MZI arms. The logical output of the proposed device depends on the light intensity (amplitude) at the output ports. Hence, the optical logic gates (XOR, XNOR, NAND, and OR) are realized by converting the input phase information to the output amplitude information. The proposed device has a low insertion loss and high extinction ratio that can be implemented as a logical device in programmable PICs for optical computing.

II. DEVICE STRUCTURE AND PRINCIPLE

A. Device structure of proposed optical logic gates

The schematic diagram of the proposed optical logic gates is shown in Fig. 1. The proposed device is composed of a cascaded 2×2 MMI coupler to form a Mach–Zehnder interferometer having an optical input at port 1 and two logical inputs “A” and “B” and logical outputs “X” and “Y” at port 2 and port 3, respectively. The general interference principle is utilized to design 2×2 MMI as a 3 dB coupler. It splits the optical light into two output ports equally, which is having $\pi/2$ phase difference between them. The thermo-optic phase shifter is implemented over the silicon nano-waveguide and is placed at both arms of MZI as PS-A and PS-B to provide logical inputs A and B, respectively. The second 2×2 MMI coupler is

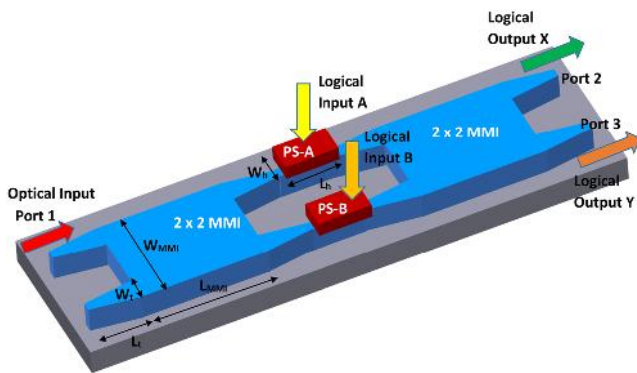


FIG. 1. Schematic diagram of the proposed reconfigurable and multifunction MMI-based optical logic gates.

also used as a 3 dB coupler. The output of the MZI structure depends on the phase difference between the two arms of MZI. The phase of the optical signal is controlled using TOPS to realize the desired logic gates.

The optical logic gates have been designed using a cascaded MMI-based Mach–Zehnder interferometer couplers and tunable thermo-optic phase shifters (TOPS). The TOPS is implemented at the two arms of MZI, which works as inputs of optical logic gates. First, we have designed and optimized an MMI-based 3 dB coupler to have minimum insertion loss and higher bandwidth. Second, we have optimized the TOPS to achieve the desired phase shift at the MZI arms. The general interference principle of the MMI is employed to design a 3 dB coupler. In general interference, first N number of images is formed at a distance $L = 3L_\pi/N$, where the beat length $L_\pi = 4n_{\text{eff}}W_{\text{MMI}}^2/3\lambda_0$, and W_{MMI} , λ_0 , and n_{eff} are the MMI width, operating wavelength, and effective index, respectively. The phase relation between the input and output optical signals in the $N \times N$ MMI waveguide is given by²⁷

$$\Phi_{ij} = \pi + \frac{\pi}{4N} (j - i)(2N - j + i) \quad \text{for } i + j \text{ even}, \quad (1)$$

$$\Phi_{ij} = \frac{\pi}{4N} (j + i - 1)(2N - j + 1) \quad \text{for } i + j \text{ odd}, \quad (2)$$

where $i = 1, 2, \dots, N$ are numbered as the bottom–top input port and $j = 1, 2, \dots, N$ are the top–bottom output port.

B. Design and optimization of MMI-based 3 dB coupler

The device structure of the MMI-based 3 dB coupler is shown in Fig. 2. The proposed structure has two input ports (1 and 4) and two output ports (2 and 3). The input and output access ports have linear tapered waveguides to minimize the reflection at the interface between the input waveguide and the multimode waveguide. We have optimized the dimension of the tapered waveguide as $W_s = 0.5 \mu\text{m}$ at one end, $W_t = 3.2 \mu\text{m}$ at the other end, and the tapered length $L_t = 30 \mu\text{m}$. The width and length of MMI are optimized using the eigenmode expansion (EME) method.

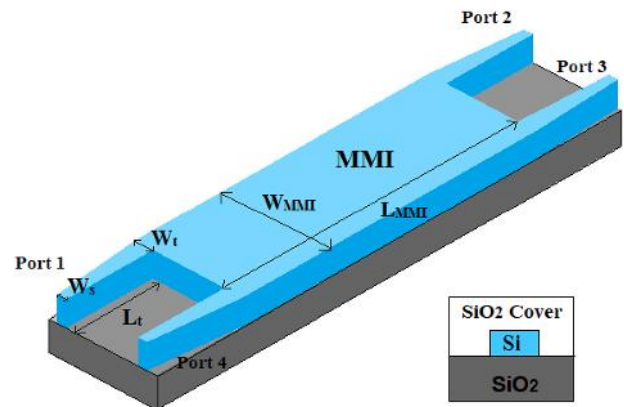
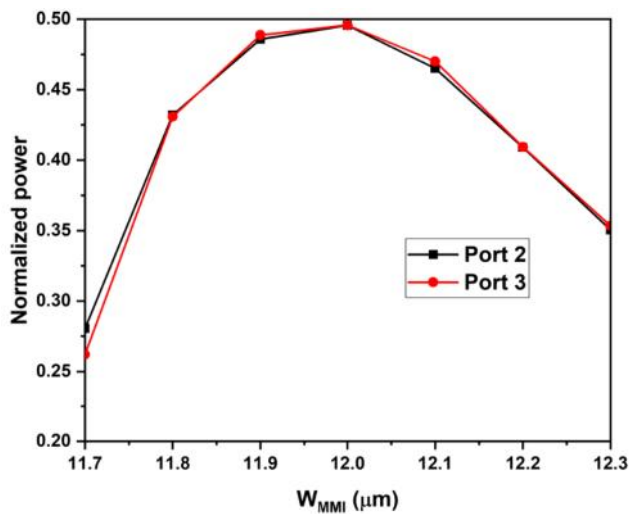
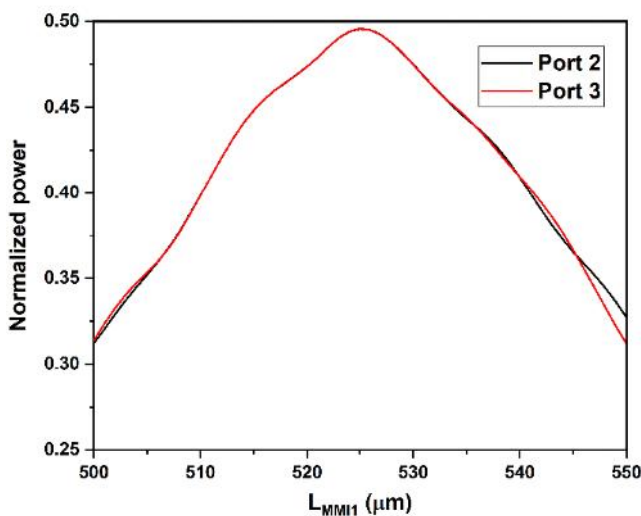


FIG. 2. Schematic diagram of the proposed MMI-based 3 dB coupler.

The transmission characteristics of the MMI coupler are analyzed for TE polarization at different MMI widths and lengths, as shown in Figs. 3(a) and 3(b), respectively. The proposed MMI-based 3 dB coupler has an MMI width (W_{MMI}) of $12\ \mu\text{m}$ and a length (L_{MMI}) of $525\ \mu\text{m}$. The maximum power is achieved at a length of $525\ \mu\text{m}$. At this length, the MMI coupler has a maximum and nearly equal normalized power of 0.5 at two output ports 2 and 3. Thus, the proposed device works efficiently as a 3 dB coupler. The fabrication tolerance (having transmission normalized power >0.9) of the 3 dB coupler is $W_{MMI} \pm 100\ \text{nm}$ and $L_{MMI} \pm 5000\ \text{nm}$.



(a)



(b)

FIG. 3. Normalized output power of the MMI-based 3 dB coupler at different (a) MMI widths and (b) MMI lengths for the TE mode.

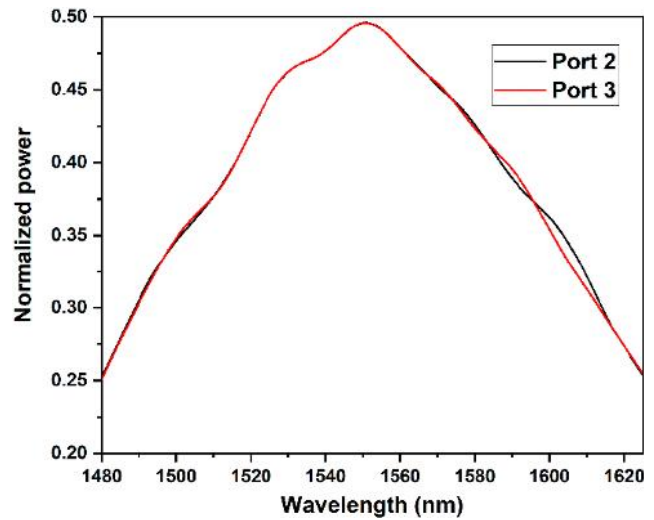


FIG. 4. Normalized output power of the MMI coupler at a different wavelength.

The transmission spectrum of the proposed 3 dB coupler is investigated for a broader wavelength, as shown in Fig. 4. We have observed that the maximum power is obtained at a wavelength of $1550\ \text{nm}$. The insertion loss of the proposed device is $0.03\ \text{dB}$ at a wavelength of $1550\ \text{nm}$ and less than $0.45\ \text{dB}$ at a wavelength of $1530\text{--}1565\ \text{nm}$ (C-band).

C. Optimization of thermo-optic phase shifter

The thermo-optic phase shifter (TOPS) is designed using the Titanium-Tungsten (TiW) alloy, and a cross-sectional view of TOPS is shown in Fig. 5. The TiW material is used in microheaters since it has a high bulk resistivity of $0.61\ \mu\Omega\ \text{m}$. The thickness of the TiW microheater (t_h) layer is chosen to be $200\ \text{nm}$, which is compatible and feasible with commercial fabrication foundries.²⁸ It is deposited over SiO_2 cladding layer of $2.2\ \mu\text{m}$. The dimension of the

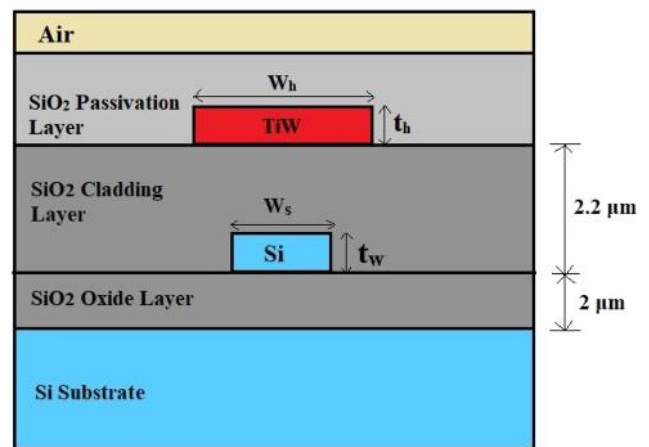


FIG. 5. Cross-sectional view of the TiW-based thermo-optic phase shifter.

microheater is a critical parameter to obtain the desired phase shift. The optical phase shift is highly sensitive to the width and length of the microheater. The TiW microheater has an optimized width (W_h) of $4 \mu\text{m}$ and length (L_h) of $200 \mu\text{m}$. The heat and temperature analysis of TOPS is performed using a numerical heat solver.²⁹

The temperature profile of TOPS is exported from the numerical device module to mode solution (finite-difference eigenmode solver) to perform optical simulations. Using this mode solver, the effective index of the silicon waveguide is analyzed at different temperatures. Due to a change in the effective index of the waveguide, the mode propagation constant gets changed. Subsequently, the phase of the optical signal is varied corresponding to the change in temperature. Thus, the thermo-optic effect can be used to tune the effective index of the silicon waveguide. The silicon waveguide has a relatively higher temperature sensitivity having a thermo-optic coefficient $dn/dT = 1.86 \times 10^{-4}$ at room temperature at a wavelength of 1550 nm .³⁰ In the proposed optical logic gates, the thermo-optic phase shifter is designed using a TiW microheater. The switching time of the tunable TOPS can be achieved below $12 \mu\text{s}$, as the TiW microheater is used to demonstrate a three-mode switch.³¹ Furthermore, the TiW heater with a doped silicon resistive heater can be used to reduce the switching time below $2.0 \mu\text{s}$.³² The phase shift (ϕ) of the TOPS can be calculated using the following equation:³³

$$\phi = \frac{2\pi}{\lambda_0} \cdot \frac{dn}{dT} \cdot \Delta T \cdot L_h, \quad (3)$$

where L_h is the length of the microheater, ΔT is the change in temperature, and λ_0 is the operating wavelength.

The phase shifts and effective indices at different microheater powers are shown in Fig. 6. It is observed that the input power of 12.3 or 61.5 mW is required to obtain a phase shift of 90° ; 24.6 , 73.8 , or 123 mW is required to obtain the phase shift of 180° ; and 36.9 or 86.1 mW is required to obtain the phase shift of 270° .

The temperature profile of the microheater for a different input power is shown in Fig. 7. The variation of temperature at the waveguide region with the microheater power is observed from the

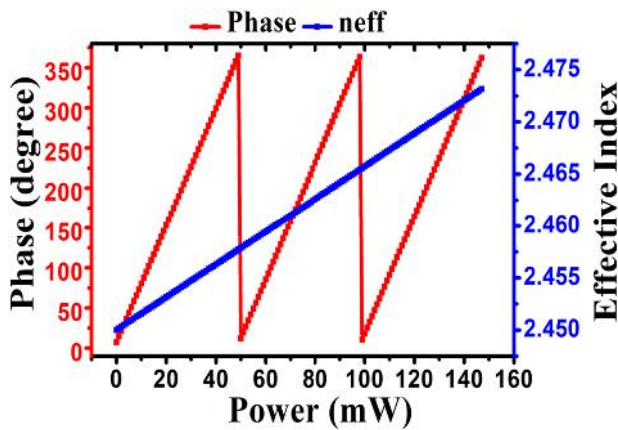


FIG. 6. Phase shift (red line) and effective index (blue line) at a different microheater power for the waveguide.

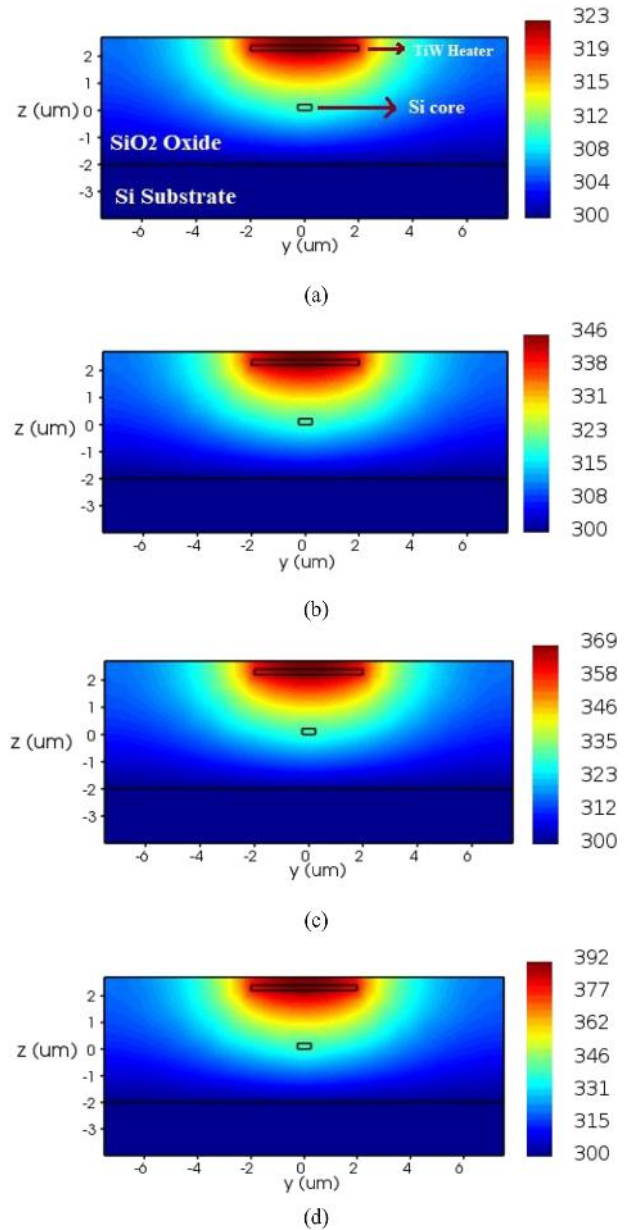


FIG. 7. The simulated temperature profile of TOPS at the different input power: (a) 12.3 mW , (b) 24.6 mW , (c) 36.9 mW , and (d) 49.2 mW .

temperature field profile. Due to the temperature change, the effective index of the waveguide gets changed. Thus, the phase of the optical signal can be tuned by varying the input microheater power.

III. SIMULATION RESULTS AND DISCUSSION

The performance of the proposed optical logic gates is analyzed through the numerical heat solver and the Eigenmode expansion

(EME) method. The proposed device works as the multifunction and reconfigurable logic gates, i.e., we can realize two logic gates simultaneously. We can also reconfigure the phase of the optical signal using TOPS to realize other logic gates. In our proposed structure, the phase information is assumed as the logical input and the amplitude of the output signal is assumed as the logical output that depends on the phase difference at the MZI arms. Thus, the input phase information is converted into the output amplitude information.

A. XOR and XNOR gates

The operational conditions and truth table of XOR and XNOR logic gates are shown in Table I. Here, we have realized two logic gates (XOR and XNOR) simultaneously. The power of TOPS is tuned to obtain the desired phase shift at the MZI arms. In the phase shifter PS-A, the power $P_A = 12.3$ mW is applied to achieve $\pi/2$ phase shift, and it corresponds to logic “0” and $P_A = 36.9$ mW is applied to achieve $3\pi/2$ phase shift, and it corresponds to logic “1.” Similarly, in the phase shifter PS-B, the phase shift of $\pi/2$ corresponds to logic “0” and the phase shift of $3\pi/2$ corresponds to logic “1.”

Case I: The phase of the optical signal at PS-A (the upper arm of MZI) is tuned to $\phi_A = \pi/2$ by applying the power $P_A = 12.3$ mW that corresponds to the logical input “0,” the phase of the optical signal at PS-B (lower arm of MZI) is tuned to $\phi_B = \pi/2$ by applying the power $P_B = 12.3$ mW that corresponds to the logical input “0,” and the logical output depends on the light intensity (amplitude) at the output ports, i.e., XOR (X) = 0 and XNOR (Y) = 1, as shown in Fig. 8(a).

Case II: The phase of the optical signal at PS-A is tuned to $\phi_A = \pi/2$ by applying the power $P_A = 12.3$ mW that corresponds to the logical input “0,” the phase of the optical signal at PS-B is tuned to $\phi_B = 3\pi/2$ by applying the power $P_B = 36.9$ mW that corresponds to the logical input “1,” and the logical output is XOR (X) = 1 and XNOR (Y) = 0, as shown in Fig. 8(b).

Case III: The phase of the optical signal at PS-A is tuned to $\phi_A = 3\pi/2$ by applying the power $P_A = 36.9$ mW that corresponds to the logical input “1,” the phase of the optical signal at PS-B is tuned to $\phi_B = \pi/2$ by applying the power $P_B = 12.3$ mW that corresponds to the logical input “0,” and the logical output is XOR (X) = 1 and XNOR (Y) = 0, as shown in Fig. 8(c).

Case IV: The phase of the optical signal at PS-A is tuned to $\phi_A = 3\pi/2$ by applying the power $P_A = 36.9$ mW that corresponds to the logical input “1,” the phase of the optical signal at PS-B is tuned to $\phi_B = 3\pi/2$ by applying the power $P_B = 36.9$ mW that corresponds to the logical input “1,” and the logical output is XOR (X) = 0 and XNOR (Y) = 1, as shown in Fig. 8(d).

TABLE I. Operation and truth table of XOR and XNOR gates.

Case	Logical input				Logical output			
	P_A (mW)	Φ_A	A	P_B (mW)	Φ_B	B	X (XOR)	Y (XNOR)
I	12.3	$\pi/2$	0	12.3	$\pi/2$	0	0	1
II	12.3	$\pi/2$	0	36.9	$3\pi/2$	1	1	0
III	36.9	$3\pi/2$	1	12.3	$\pi/2$	0	1	0
IV	36.9	$3\pi/2$	1	36.9	$3\pi/2$	1	0	1

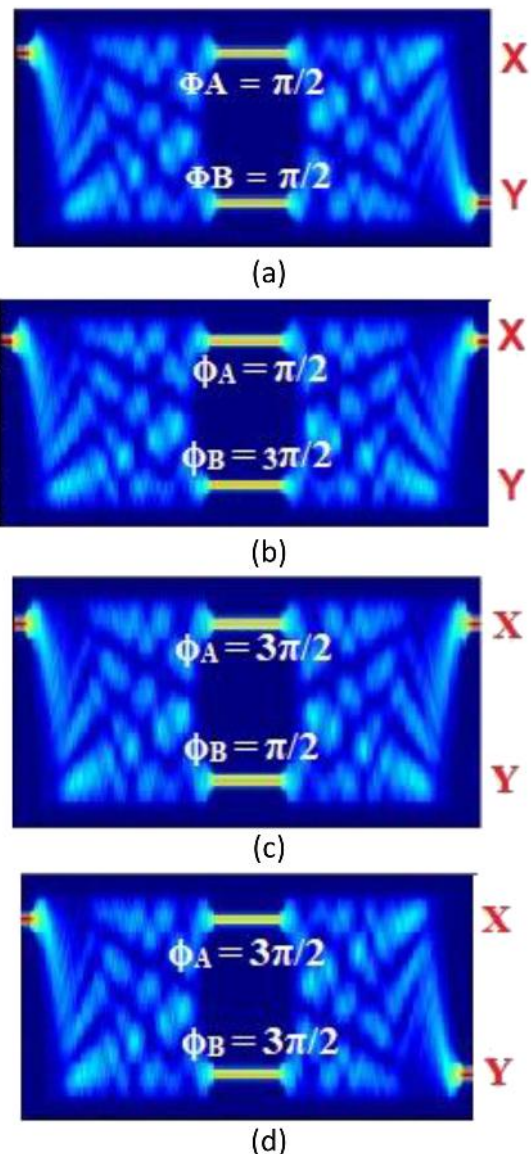


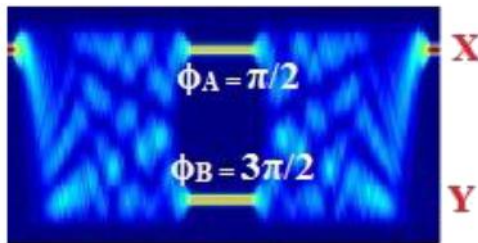
FIG. 8. Simulated optical intensity profile of XOR and XNOR gate: (a) Case I, (b) case II, (c) case III, and (d) case IV.

B. NAND and OR gates

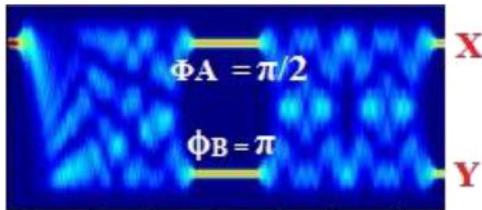
The operational conditions and truth table of the NAND and OR logic gates are shown in Table II. Here, we have realized two logic gates (NAND and OR) simultaneously. In the phase shifter PS-A, the power $P_A = 61.5$ mW is applied to achieve a phase shift of $\pi/2$ and it corresponds to logic “0,” and $P_A = 73.8$ mW is applied to achieve a phase shift of π and it corresponds to logic “1.” Similarly, in the phase shifter PS-B, power $P_B = 86.1$ mW is applied to achieve $3\pi/2$ phase shift and it corresponds to logic “0,” and $P_B = 123$ mW is applied to achieve π phase shift and it corresponds to logic “1.”

TABLE II. Operation and truth table of NAND and OR gates.

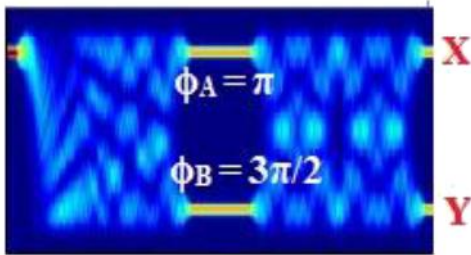
Case	Logical input					Logical output		
	P_A (mW)	Φ_A	A	P_B (mW)	Φ_B	B	X (NAND)	Y (OR)
I	61.5	$\pi/2$	0	86.1	$3\pi/2$	0	1	0
II	61.5	$\pi/2$	0	123.0	π	1	1	1
III	73.8	π	1	86.1	$3\pi/2$	0	1	1
IV	73.8	π	1	123.0	π	1	0	1



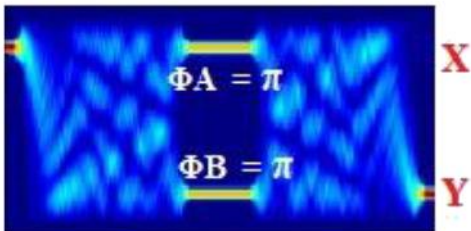
(a)



(b)



(c)



(d)

FIG. 9. Simulated optical intensity profile of NAND and OR gate: (a) Case I, (b) Case II, (c) Case III, and (d) Case IV.

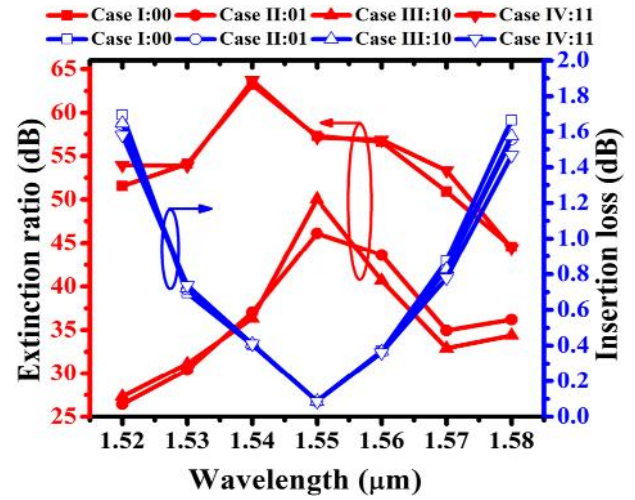


FIG. 10. Extinction ratio (red lines) and insertion loss (blue lines) of the XOR and XNOR gates as a function of wavelength.

Case I: The microheater power is tuned to $P_A = 61.5$ mW for the phase shift $\Phi_A = \pi/2$ that corresponds to the logical input “0” and $P_B = 86.1$ mW for the phase shift $\Phi_B = 3\pi/2$ that corresponds to the logical input “0,” and the logical output is NAND (X) = “1” and OR (Y) = “0,” as shown in Fig. 9(a).

Case II: The microheater power is tuned to $P_A = 61.5$ mW for the phase shift $\Phi_A = \pi/2$ that corresponds to the logical input “0” and $P_B = 123$ mW for the phase shift $\Phi_B = \pi$ that corresponds to the logical input “1,” and the logical output is NAND (X) = “1” and OR (Y) = “1,” as shown in Fig. 9(b).

Case III: The microheater power is tuned to $P_A = 73.8$ mW for the phase shift $\Phi_A = \pi$ that corresponds to the logical input “1” and

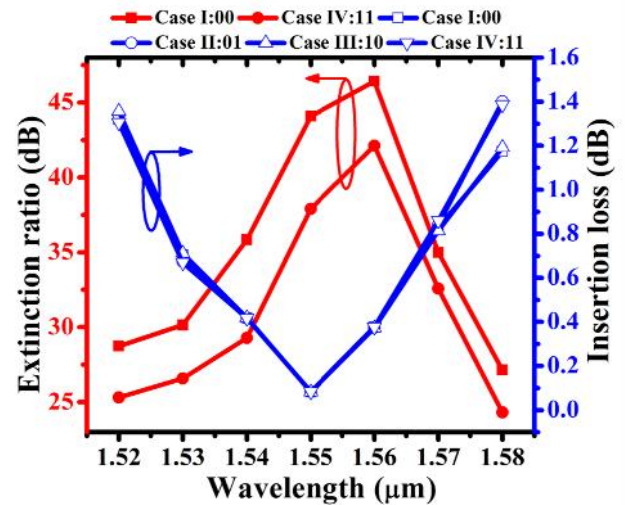


FIG. 11. Extinction ratio (red lines) and insertion loss (blue lines) of NAND and OR gate as a function of wavelength.

TABLE III. Comparison of the proposed work with the reported optical logic gates.

References	Device	Technology	Logical function	Insertion loss (dB)	ER (dB)
16	Rectangular ring resonator	Graphene nanoribbon	NOT, XOR, and XNOR	...	14.2, 19.5, and 14.1
17	Y-splitter	Hybrid plasmonic waveguide	OR, XOR, NOT	...	26
18	Multi-functional plasmonic waveguide	Angle manipulation	AND, NAND, NOR, and NOT	...	12.9, 24.2, 4.5, and 24.2
19	Phase-shifted grating	Cross-phase modulation	NOT, AND, NAND, XOR, and XNOR	...	>5
20	Photonic crystal	Nonlinear Kerr effect	XOR, XNOR, NAND and NOT	...	25, 30, 37 and 20.7
21	MMI-based optical logic gates	Photonic crystal	XOR, XNOR, NAND, and OR	<0.3 for C band	28.6, 28.6, 25 and 26.6 for C band
22	Multimode interference (multilogic)	Semi-binary-phase shift-keyed	XOR, NAND, OR, XNOR, and NOT	<0.14 for C band	26, 24.7, 25.9, 26, and 25 dB
24	Reconfigurable optical logic architecture (microring resonator)	Electro-optic principle	AND, OR, XOR, and XNOR	~0.15 dB at 1549.1 nm	>10
This work	MMI-based MZI (Reconfigurable and multifunction)	Thermo-optic phase shifter	XOR, XNOR, NAND, and OR	0.09 at 1550 nm <0.8 dB for C band	>37 at 1550 nm >25 for C band

$P_B = 86.1$ mW for the phase shift $\phi_B = 3\pi/2$ that corresponds to the logical input “0,” and the logical output is NAND ($X = “1”$) and OR ($Y = “1,”$ as shown in Fig. 9(c).

Case IV: The microheater power is tuned to $P_A = 73.8$ mW for the phase shift $\phi_A = \pi$ that corresponds to the logical input “1” and $P_B = 123$ mW for the phase shift $\phi_B = \pi$ that corresponds to the logical input “1,” and the logical output is NAND ($X = “0”$) and OR ($Y = “1,”$ as shown in Fig. 9(d).

The on-off extinction ratio (ER) is a significant parameter to analyze the performance of optical logic gates. The extinction ratio and insertion loss (IL) of XOR and XNOR logic gates have been investigated by varying the input wavelengths for different cases, as shown in Fig. 10. The proposed XOR and XNOR logic gates have an ER of >45 dB and IL of 0.08 dB at a 1550 nm wavelength, and ER of >25 dB and IL < 0.8 dB for the C-band window (1530–1565 nm).

Figure 11 shows the ER and IL of NAND and OR logic gates at different wavelengths. It is observed that the proposed NAND and OR logic gates have an ER of >37 dB and IL of 0.09 dB at a 1550 nm, and an ER of >25 dB and IL of <0.8 dB for the C-band. A comparative performance analysis of various optical logic gates is shown in Table III. Compared with other structures, the proposed device shows competitive results.

IV. CONCLUSION

In this paper, optical logic gates (XOR, XNOR, NAND, and OR) are demonstrated by using a cascaded 2×2 MMI and thermo-optic phase shifter in a MZI configuration. The simulation results show that the proposed logic device has an insertion loss of <0.8 dB and an on-off extinction ratio of >25 dB for the C-band window. The proposed device works as a reconfigurable and multifunction device by properly adjusting the phase of the optical signal with

TOPS. The proposed optical logic gates can be a useful logical device in programmable photonic integrated circuits for optical computing.

ACKNOWLEDGMENTS

This research was supported by the Science and Engineering Research Board (SERB), Department of Science and Technology (DST), Government of India, under Grant No. 2019/000373.

AUTHOR DECLARATIONS

Conflict of Interest

The authors have no conflicts to disclose.

DATA AVAILABILITY

The data that support the findings of this study are available within the article.

REFERENCES

- W. Bogaerts and A. Rahim, “Programmable photonics: An opportunity for an accessible large-volume PIC ecosystem,” *IEEE J. Sel. Top. Quantum Electron.* **26**(5), (2020).
- D. Chack and S. Hassan, *Opt. Eng.* **59**, 105102 (2020).
- K. Suzuki, R. Konoike, S. Suda, H. Matsuura, S. Namiki, H. Kawashima, and K. Ikeda, *J. Lightwave Technol.* **38**, 233 (2020).
- C. Feng, Z. Ying, Z. Zhao, R. Mital, D. Z. Pan, and R. T. Chen, *IEEE J. Sel. Top. Quantum Electron.* **26**, 8302208 (2020).
- Y. Shen, X. Meng, Q. Cheng, S. Rumley, N. Abrams, A. Gazman, E. Manzhosov, M. S. Glick, and K. Bergman, *J. Lightwave Technol.* **37**, 245 (2019).
- W. Dong, L. Lei, L. Chen, Y. Yu, and X. Zhang, *J. Lightwave Technol.* **38**, 5586 (2020).
- H. Yang, V. Khayrudinov, V. Dhaka, H. Jiang, A. Autere, H. Lipsanen, Z. Sun, and H. Jussila, *Sci. Adv.* **4**, eaar7954 (2018).

- ⁸Z. Ying, S. Dhar, Z. Zhao, C. Feng, R. Mital, C. J. Chung, D. Z. Pan, R. A. Soref, and R. T. Chen, *IEEE J. Sel. Top. Quantum Electron.* **24**, 7600310 (2018).
- ⁹R. Athale and D. Psaltis, *Opt. Photonics News* **27**, 32 (2016).
- ¹⁰V. Dhasarathan, S. K. Sahu, T. K. Nguyen, and G. Palai, *Optik* **202**, 163723 (2020).
- ¹¹W. Bogaerts, D. Pérez, J. Capmany, D. A. B. Miller, J. Poon, D. Englund, F. Morichetti, and A. Melloni, *Nature* **586**, 207 (2020).
- ¹²Z. Ying, C. Feng, Z. Zhao, R. Soref, D. Pan, and R. T. Chen, *Appl. Phys. Lett.* **115**, 171104 (2019).
- ¹³A. Politi, J. C. F. Matthews, M. G. Thompson, and J. L. O'Brien, *IEEE J. Sel. Top. Quantum Electron.* **15**, 1673 (2009).
- ¹⁴A. Kotb and C. Guo, *Opt. Laser Technol.* **137**, 106828 (2021).
- ¹⁵A. Godbole, P. P. Dali, V. Janyani, T. Tanabe, and G. Singh, *IEEE J. Sel. Top. Quantum Electron.* **22**, 326 (2016).
- ¹⁶W. Su and Z. Geng, *IEEE Photonics J.* **10**, 5900608 (2018).
- ¹⁷P. Sharma and V. D. Kumar, *IEEE Photonics Technol. Lett.* **30**, 959 (2018).
- ¹⁸Y. Ye, Y. Wang, Y. Xie, T. Song, B. Liu, J. Chai, and Y. Liu, *IEEE Trans. Nanotechnol.* **19**, 94 (2020).
- ¹⁹Q. Li, J. Song, X. Chen, M. Bi, M. Hu, and S. Li, *Appl. Opt.* **55**, 6880 (2016).
- ²⁰Z. Mohebbi, N. Nozhat, and F. Emami, *Opt. Commun.* **355**, 130 (2015).
- ²¹W. Liu, D. Yang, G. Shen, H. Tian, and Y. Ji, *Opt. Laser Technol.* **50**, 55 (2013).
- ²²S. Mohammadnejad, Z. F. Chaykandi, and A. Bahrami, *IEEE J. Quantum Electron.* **50**, 1 (2014).
- ²³Y. Ishizaka, Y. Kawaguchi, K. Saitoh, and M. Koshiba, *J. Lightwave Technol.* **29**, 2836 (2011).
- ²⁴C. Qiu, X. Ye, R. Soref, L. Yang, and Q. Xu, *Opt. Lett.* **37**, 3942 (2012).
- ²⁵Q. Li, M. Zhu, D. Li, Z. Zhang, Y. Wei, M. Hu, X. Zhou, and X. Tang, *Appl. Opt.* **53**, 4708 (2014).
- ²⁶Y. Xie, Y. Shi, L. Liu, J. Wang, R. Priti, G. Zhang, O. Liboiron-Ladouceur, and D. Dai, *IEEE J. Sel. Top. Quantum Electron.* **26**, 3600220 (2020).
- ²⁷M. Bachmann, P. A. Besse, and H. Melchior, *Appl. Opt.* **33**, 3905 (1994).
- ²⁸See <https://www.appliednt.com/nanosoi-fabrication-service/> for Applied Nano tools, Inc. Canada.
- ²⁹See <https://www.lumerical.com/products/heat/> for lumerical heat solver software.
- ³⁰S. Sabouri, L. A. Mendoza, M. Catuneanu, M. Namdari, and K. Jamshidi, *IEEE Photonics J.* **13**, 6600112 (2021).
- ³¹R. B. Priti, G. Zhang, and O. Liboiron-Ladouceur, *Opt. Express* **27**, 14199 (2019).
- ³²R. B. Priti, Y. Xiong, and O. Liboiron-Ladouceur, in *2016 IEEE Photonics Conference IPC 2016* (IEEE, 2017).
- ³³N. C. Harris, Y. Ma, J. Mower, T. Baehr-Jones, D. Englund, M. Hochberg, and C. Galland, *Opt. Express* **22**, 10487 (2014).